nature genetics

ARTICLES

https://doi.org/10.1038/s41588-019-0503-y

Natural variation in *ZmFBL41* confers banded leaf and sheath blight resistance in maize

Ning Li[1], Bao Lin[1], Hong Wang[2,4], Xiaoming Li[1], Fangfang Yang[1], Xinhua Ding[1,3], Jianbing Yan[2] and Zhaohui Chu[1*]

Rhizoctonia solani **is a widely distributed phytopathogen that causes banded leaf and sheath blight in maize and sheath blight in rice. Here, we identified an F-box protein (ZmFBL41) that confers resistance to banded leaf and sheath blight through a genome-wide association study in maize. Rice overexpressing *ZmFBL41* showed elevated susceptibility to *R. solani*. Two amino acid substitutions in this allele prevent its interaction with ZmCAD, which encodes the final enzyme in the monolignol biosynthetic pathway, resulting in the inhibition of ZmCAD degradation and, consequently, the accumulation of lignin and restriction of lesion expansion. Knocking out the *ZmCAD*-homologous gene *OsCAD8B* in rice enhanced susceptibility to *R. solani*. The results reveal a susceptibility mechanism in which *R. solani* targets the host proteasome to modify the secondary metabolism of the plant cell wall for its invasion. More importantly, it provides an opportunity to generate *R. solani*–resistant varieties of different plant species.**

Maize is one of the important crops grown for food, feed and fuel, but maize production is often affected by the frequent occurrence of extreme weather and epidemics of major maize diseases. Therefore, there is a need for new maize varieties with strong disease resistance, high yield and good quality[1]. Traditional hybrid breeding is often faced with problems of long breeding cycles and low selection efficiency, which restrict the quality and speed of maize breeding[2]. Thus, improving maize by biotechnology is an effective method. Because most economic traits in maize are quantitative traits that are usually controlled by polygenes and interactions among genes and/or genes and the environment[3], an appropriate approach to locating quantitative trait loci (QTLs) is necessary.

Genome-wide association study (GWAS) is an effective method for fine-mapping the QTLs that underlie complex traits based on linkage disequilibrium (LD)[4]. This association mapping strategy was first proposed[5] in 1996 and has been mainly applied to the analysis of complex traits associated with human diseases[6]. In recent years, GWAS has been widely used in the genetic dissection of complex traits in crops, and many QTLs associated with agriculturally important traits in crops have been identified[7–12]. In maize, several cloned genes and proposed gene candidates for disease resistance have been comprehensively studied using a GWAS approach[13–17]. These advances suggest that GWAS is a powerful tool to effectively and efficiently identify genome–phenotype associations.

Banded leaf and sheath blight (BLSB) in maize, which is caused by the necrotrophic fungus *R. solani*, is an important disease in China as well as in south and southeast Asia[18]. Furthermore, rice sheath blight, which is caused by the same pathogen, is the most destructive disease in rice[19]. Although maize varieties that are relatively resistant to *R. solani* have been identified, no completely field-resistant or immune maize cultivar has been found[18]. Therefore, mining resistance resources and understanding the genetic mechanisms of maize resistance to *R. solani* will greatly benefit BLSB resistance breeding. Studies have shown that resistance to *R. solani* is a quantitative trait controlled by multiple genes, and no major genes confer resistance to *R. solani*[20,21]. To date, a number of resistant QTLs and defense-related genes have been identified and functionally characterized[22–26]. However, the mechanisms of maize or rice resistance to *R. solani* and the pathogenesis of *R. solani* are poorly understood.

Protein degradation mediated by E3 ubiquitin ligases is an important process that has critical roles in the regulation of the immune response, and several proteins with E3 ligase activity have been demonstrated to function in regulating the innate immune response in plants[27–29]. The SKP1–cullin–F-box (SCF) complex is a subfamily of E3 ligases, and substrate recognition is provided by the F-box protein in this complex[30]. Additionally, the role of F-box proteins in plant immunity has been well studied[31,32].

Here, we report the isolation and mechanistic characterization of a novel allele, *zmfbl41*, involved in maize resistance to *R. solani*. *ZmFBL41* encodes an F-box protein, that interacts with the cinnamyl alcohol dehydrogenase ZmCAD, leading to the ubiquitination and degradation of ZmCAD. ZmCAD accumulation in *zmfbl41* plants results in enhanced BLSB resistance. Thus, we reveal a mechanism by which the ZmFBL41–ZmCAD interaction regulates maize BLSB resistance.

Results

GWAS of BLSB resistance in maize inbred lines. To investigate maize resistance to *R. solani*, BLSB resistance was indexed by lesion length at 5 d post-inoculation (d.p.i.) with *R. solani* in a maize natural-variation population (318 different inbred lines) in the field (Supplementary Table 1). This population includes 133 tropical or subtropical inbred lines, 78 temperate lines and 71 lines of mixed origin[33]. Large variations in lesion length were observed in the phenotypic assays, with average lesion lengths ranging from 0.8 cm to 14.13 cm (Supplementary Fig. 1a). Among the different genetic resources, the tropical/subtropical subpopulation exhibited the greatest BLSB resistance (Supplementary Fig. 1b). To investigate

[1]State Key Laboratory of Crop Biology, College of Agronomy, Shandong Agricultural University, Taian, China. [2]National Key Laboratory of Crop Genetic Improvement, Huazhong Agricultural University, Wuhan, China. [3]Shandong Provincial Key Laboratory for Biology of Vegetable Disease and Insect Pests, College of Plant Protection, Shandong Agricultural University, Taian, China. [4]Present address: Key Laboratory of Northern China Crop Germplasm Resources, College of Agronomy, Hebei Agricultural University, Baoding, China. *e-mail: zchu@sdau.edu.cn

the repeatability of the phenotype among different lines, we randomly selected five resistant haplotypes (RH) and five susceptible haplotypes (SH) and determined the disease index at 14 d.p.i. in the field. The repeatability of the phenotype was significantly correlated ($r^2 = 0.9795$, $P = 5.06 \times 10^{-6}$; Supplementary Fig. 2). Using 542,438 SNPs (http://www.maizego.org/Resources.html) with a minor allele frequency of ≥0.05 covering the whole maize genome[8,34], a GWAS was performed for BLSB resistance using the general linear model (GLM) approach controlling population structure and identified 28 SNPs above the suggestive significance threshold of association ($P < 1 \times 10^{-5}$; Fig. 1a and Supplementary Fig. 1c). These significant SNPs correspond to nine loci located on chromosomes 1, 4, 7 and 8; candidate genes are listed in Supplementary Table 2.

***ZmFBL41* is significantly associated with BLSB resistance.** The most significant SNP chr4.S_180199219 ($P < 1.84 \times 10^{-6}$) is located within the second exon of a single gene (*GRMZM2G109140*) residing on chromosome 4 (Fig. 1b). *GRMZM2G109140* is predicted to encode an F-box protein with a molecular mass of 41 kDa (Supplementary Fig. 3a) that shares 79% protein sequence identity[35] with OsFBX61 in rice. Thus, we designated the gene *ZmFBL41*. A subcellular localization assay suggests that ZmFBL41 localizes to the cytoplasm (Supplementary Fig. 3b). We subsequently resequenced alleles of *ZmFBL41* from 28 SH lines (lesion length > 7 cm) and 23 RH lines (lesion length < 5 cm), including 398 bp upstream of the 5′ untranslated region (UTR), 1,338 bp 5′ UTR, 264 bp 3′ UTR and 1,190 bp downstream of the 3′ UTR. Five insertions and deletions (indels) were identified upstream of the translation start codon (ATG) and were not associated with BLSB resistance (Fig. 2a and Supplementary Table 3). Moreover, comparative analysis of the $ZmFBL41^{SH}$ and $ZmFBL41^{RH}$ sequences showed that four SNPs distributed in the second exon region were in strong LD with the lead SNP 2867 ($r^2 > 0.8$) (Fig. 2a).

The 51 maize inbred lines were classified into two haplotype groups based on these five variants (frequency > 0.01) (Fig. 2b). $ZmFBL41^{B73}$ is a representative of haplotype 1, whereas $ZmFBL41^{Chang7\text{-}2}$ belongs to haplotype 2. Statistically, lines with haplotype 1 had significantly longer lesions than those with haplotype 2 ($P = 4.68 \times 10^{-19}$). Therefore, we designated haplotype 1 and haplotype 2 as susceptible and resistant alleles of *ZmFBL41*, respectively (Fig. 2b). As five indels are located in the promoter region, we randomly selected 20 SH and 17 RH lines to measure the expression level of *ZmFBL41* after inoculation with *R. solani*. We did not detect any significant differences in *ZmFBL41* expression between the SH and RH lines (Fig. 2c and Supplementary Table 4), suggesting that the susceptible and resistant phenotypes of BLSB resistance in the two *ZmFBL41* haplotypes are independent of the transcriptional level.

***ZmFBL41*^{B73} is a negative regulator of *R. solani* in maize.** To assess the involvement of *ZmFBL41* in maize resistance to *R. solani*, we identified a maize transposon-insertion line, *zmfbl41*, from the maize UniformMu resource, which carried a *Mutator* insertion (mu1059763) in the 5′ UTR of *ZmFBL41* (Supplementary Fig. 4a,b). The expression level of *ZmFBL41* in the *zmfbl41* line was reduced to 28% of that in the maize inbred line W22 (Supplementary Fig. 4c). The *zmfbl41* line was inoculated with *R. solani* along with the W22 line in the field, and the disease index was counted 14 d.p.i. The *zmfbl41* line exhibited weaker disease symptoms than W22 after *R. solani* infection; the disease index of *zmfbl41* was reduced by approximately 29% compared to that of W22 (Fig. 3a). Moreover, the expression levels of *ZmPR4* (*GRMZM2G117942*) and *ZmPR10* (*GRMZM2G112488*) were much higher in *zmfbl41* than in W22 after *R. solani* infection (Fig. 3b).

Because rice is infected by *R. solani* in addition to maize, we proposed that expression of the susceptible allele of *ZmFBL41* could promote rice susceptibility to *R. solani*. We generated transgenic rice plants expressing the cDNA of $ZmFBL41^{B73}$ in Zhonghua 11. The *ZmFBL41* RNA levels were tested in three independent $ZmFBL41^{B73}$-overexpressing lines in the T_1 generation (Supplementary Fig. 4d). At 7 d.p.i. with *R. solani*, the three $ZmFBL41^{B73}$-overexpressing lines had developed longer lesions, and the lesion length was between 3.5 and 7.3 cm longer than that in Zhonghua 11 (Fig. 3c). Additionally, detection of the expression levels of *OsPR1* (*LOC_Os07g03730*), *OsPR5* (*LOC_Os12g43380*) and *OsPR10* (*LOC_Os03g18850*) showed that the expression of these *PR* genes was significantly reduced compared to those in Zhonghua 11 after *R. solani* infection (Fig. 3d). Thus, the results of the mutation and overexpression experiments strongly suggest that $ZmFBL41^{B73}$ functions as a negative regulator of BLSB resistance.

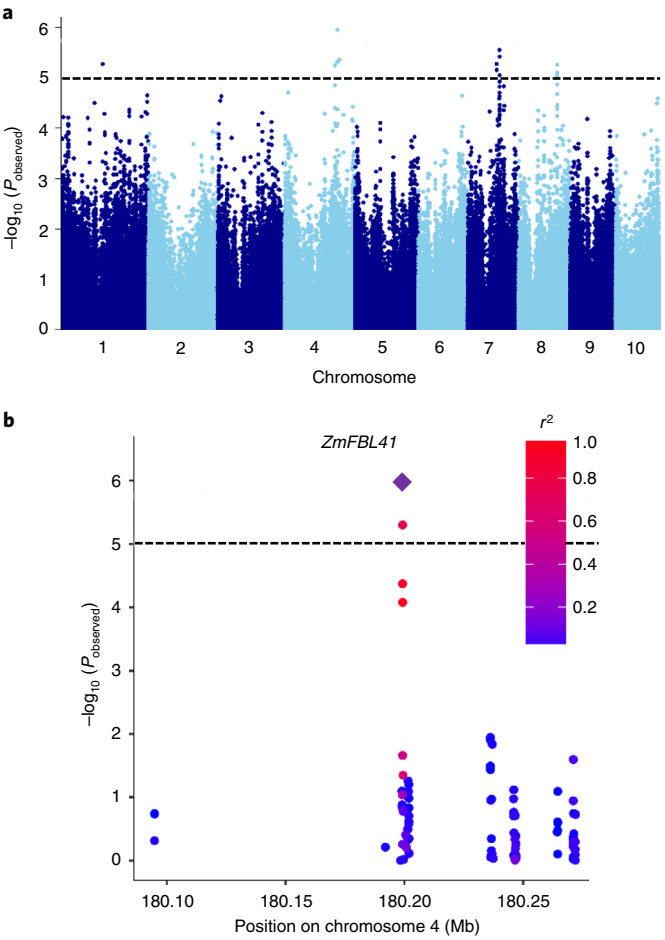

Fig. 1 | GWAS for BLSB resistance in maize. a, Manhattan plot of the GWAS. The dashed horizontal line depicts the Bonferroni-adjusted significance threshold ($P = 1.0 \times 10^{-5}$). **b**, Regional Manhattan plot of the *ZmFBL41* genomic region on chromosome 4. The 0.1-Mb genomic region on either side of the most significant SNP is shown. The lead SNP is shown with a purple diamond, and the other SNPs are colored according to their LD (r^2 value) with the lead SNP.

ZmFBL41^{B73} is a component of the SCF^{ZmFBL41} complex. The F-box protein usually interacts with the S-phase kinase-associated protein 1 (SKP1) through its F-box domain and forms the SCF E3 ubiquitin ligase complex[36,37]. ZmFBL41^{B73} contains an F-box domain in its N-terminal region (amino acids 13–60) (Supplementary Fig. 3a). We therefore tested whether ZmFBL41^{B73} interacts with SKP1 proteins. We first constructed the ZmFBL41^{B73} bait vector and two deletion vectors of ZmFBL41^{B73}, one of which lacked the leucine-rich

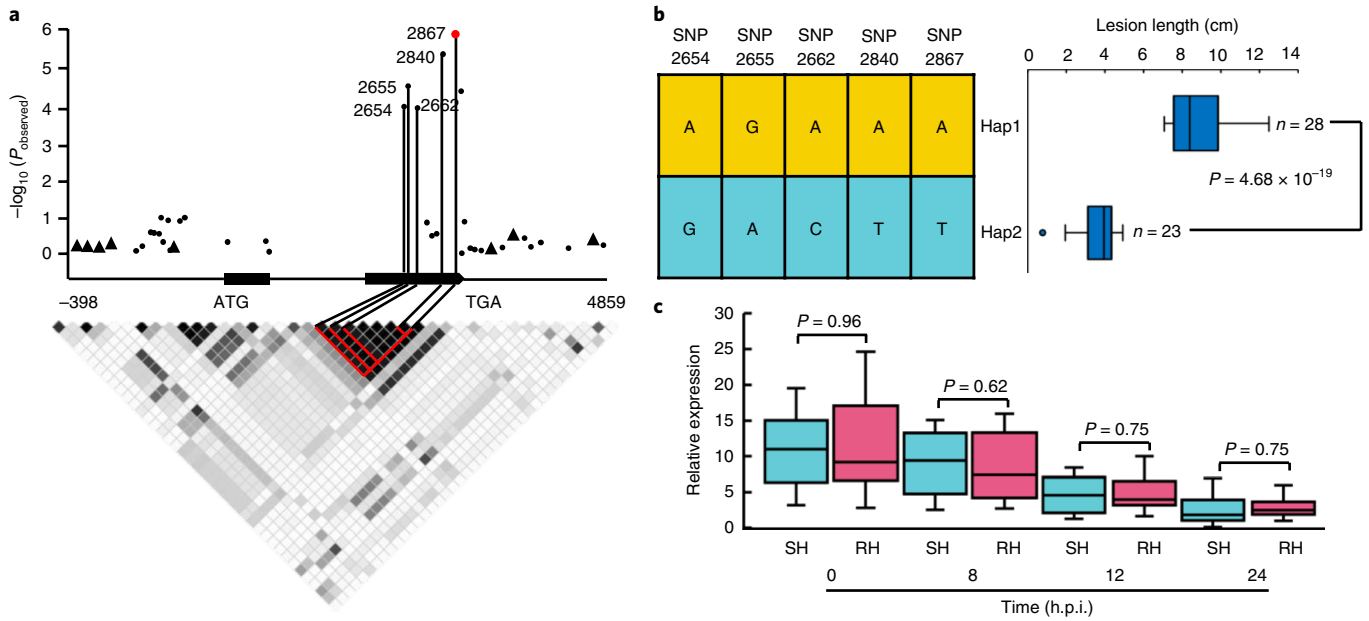

Fig. 2 | Natural variations in *ZmFBL41* were significantly associated with maize resistance to *R. solani*. **a**, *ZmFBL41*-based association mapping and pairwise LD analysis. Triangles denote indels and dots represent SNPs. The lead SNP is highlighted in red. The SNPs showing strong LD with the lead SNP are connected to the pairwise LD diagram with solid lines and highlighted with red lines. **b**, Haplotypes (Hap) of *ZmFBL41* among maize natural variations. *n* denotes the number of genotypes belonging to each haplotype group. Statistical significance was determined using a two-sided *t*-test. The lesion-length distribution of each haplotype group is displayed as a box plot. **c**, Comparison of *ZmFBL41* expression between the SH and RH lines. Gene expression levels were determined among 20 SH lines and 17 RH lines during *R. solani* infection. In box plots, center values are medians, solid lines indicate variability outside the upper and lower quartiles and dots denote outliers. Statistical significance was determined using a Student's two-sided *t*-test.

repeat (LRR) domain (ZmFBL41^{B73}ΔLRR) and the other lacking the F-box domain (ZmFBL41^{B73}ΔF-box) (Supplementary Fig. 5a). The interactions between ZmFBL41^{B73} and six candidate ZmSKP1-like proteins were confirmed by a yeast two-hybrid assay (Y2H). The results demonstrated that ZmFBL41^{B73} and ZmFBL41^{B73}ΔLRR could interact with ZmSKP1–1 (GRMZM2G417092) rather than with five other ZmSKP1-like proteins, whereas ZmFBL41^{B73}ΔF-box could not interact with any of the six ZmSKP1-like proteins (Supplementary Fig. 5b). To test whether ZmFBL41^{B73} and ZmSKP1-1 interact in vivo, we performed a co-immunoprecipitation assay after transiently expressing Myc-tagged ZmSKP1-1 (ZmSKP1-1–Myc) and HA-tagged ZmFBL41^{B73} (ZmFBL41^{B73}–HA) or ZmFBL41^{B73}ΔLRR (ZmFBL41^{B73}ΔLRR–HA) in *Nicotiana benthamiana*. We found that an anti-Myc antibody could co-immunoprecipitate ZmFBL41^{B73}–HA as well as ZmFBL41^{B73}ΔLRR–HA (Supplementary Fig. 5c). Furthermore, a bimolecular fluorescence complementation (BiFC) assay showed that ZmFBL41^{B73} and ZmFBL41^{B73}ΔLRR interacted with ZmSKP1-1 in *N. benthamiana* cells (Supplementary Fig. 5d). Together, these results demonstrate that ZmFBL41^{B73} interacts with ZmSKP1 in planta and is a component of the SCF^{ZmFBL41} E3 ubiquitin ligase complex.

ZmCAD interacts with ZmFBL41^{B73}. The SCF E3 ubiquitin ligase complex has been reported to recruit substrates through the LRR or WD40 domain of the F-box proteins, after which the substrates are degraded by the 26S proteasome[36–38]. ZmFBL41^{B73} is a negative regulator of BLSB resistance by degrading a target protein associated with resistance factors (Fig. 3). To reveal the target of ZmFBL41^{B73}, we screened for ZmFBL41^{B73}LRR-interacting proteins using a Y2H assay with a cDNA library prepared from maize challenged with *R. solani*. Among the potential interacting genes, one gene (*GRMZM2G700188*) was particularly interesting as it encodes a cinnamyl alcohol dehydrogenase (annotated as ZmCAD). The interaction between ZmFBL41^{B73}LRR and ZmCAD was first confirmed by Y2H assay; moreover, ZmFBL41^{B73}ΔLRR could not interact with ZmCAD (Fig. 4a). To determine the specific interaction between ZmCAD and ZmFBL41^{B73}, we performed the interaction experiment with another maize F-box protein with a LRR domain, ZmFBX252.2 (GRMZM2G330526), in yeast. The results showed that ZmFBX252.2 could not interact with ZmCAD (Fig. 4a). The interaction was further validated by immunoprecipitation and BiFC in *N. benthamiana* (Fig. 4b,c). Together, these results demonstrate that ZmFBL41^{B73} interacts with ZmCAD in planta.

ZmFBL41^{B73} targets ZmCAD for ubiquitination and degradation. We next examined the degradation of ZmCAD in maize cell extracts using a cell-free system as reported previously[39]. As shown in Fig. 4d, MG132 (a proteasome inhibitor) treatment delayed the degradation of ZmCAD, indicating that ZmCAD was degraded by the 26S proteasome. Furthermore, we found that ZmCAD showed delayed degradation in *zmfbl41* mutant plants compared with wild-type plants (Fig. 4e), suggesting that the degradation of ZmCAD is dependent on ZmFBL41^{B73}. To further confirm that ZmCAD is a substrate of ZmFBL41^{B73} for degradation, we performed a degradation assay using a transient expression system in *N. benthamiana*. A higher accumulation of ZmCAD–HA was observed in the MG132-treated leaves (Fig. 4f), indicating that ZmCAD is more stable when proteasome activity is inhibited. Furthermore, the reduction in ZmCAD–HA accumulation induced by *ZmFBL41*^{B73} overexpression was suppressed by MG132 (Fig. 4f), suggesting that the degradation of ZmCAD is partially dependent on ZmFBL41^{B73}. Together, these findings demonstrate that ZmCAD and ZmFBL41^{B73} form a protein module and that the SCF^{ZmFBL41} complex controls the steady state of ZmCAD.

***ZmCAD* positively regulates maize resistance to *R. solani*.** To assess the role of *ZmCAD* in BLSB resistance, we identified a maize transposon-insertion line, *zmcad*, from the maize UniformMu

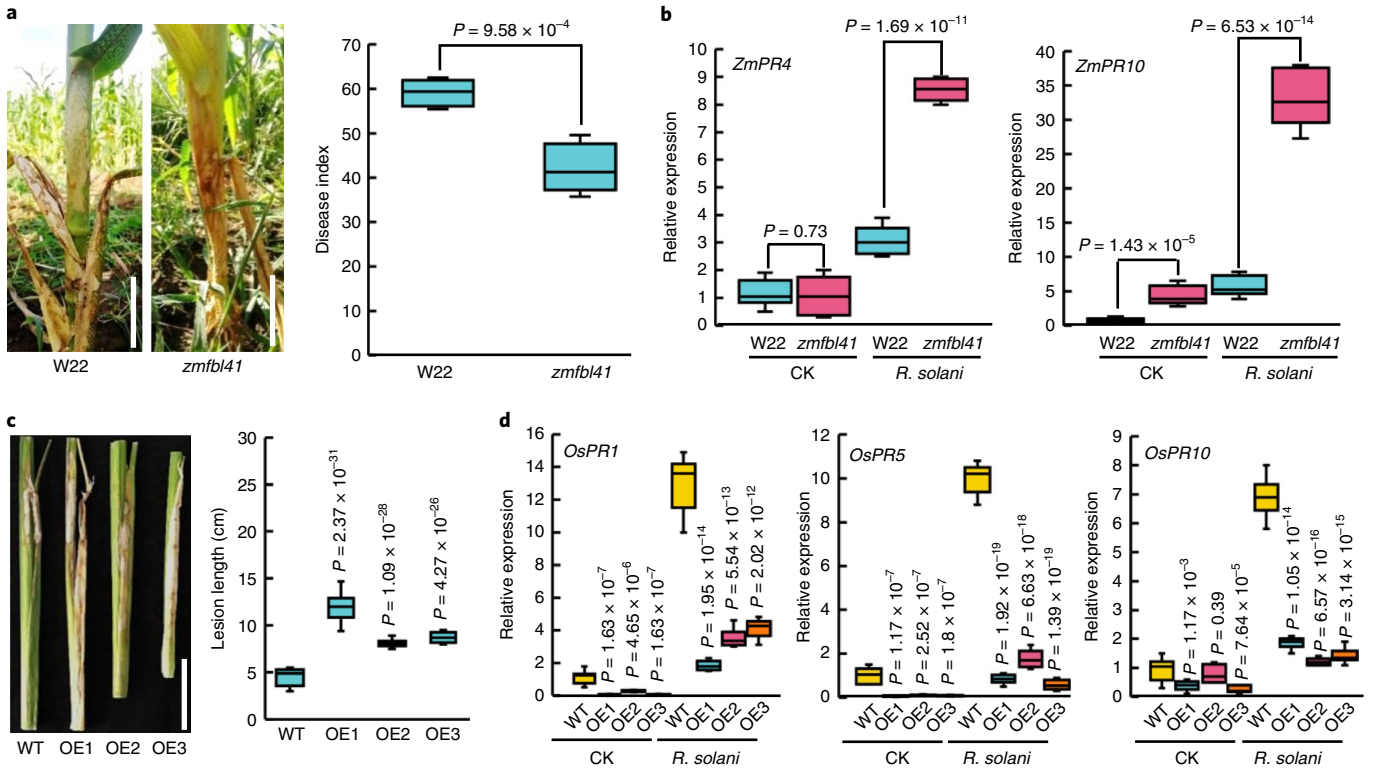

Fig. 3 | Function of *ZmFBL41* in BLSB resistance. a, Resistant phenotype of the *zmfbl41* transposon-insertion line. An inoculated *zmfbl41* transposon-insertion line in the field is shown. The disease index was counted from 10 plants of each line at 14 d.p.i. Independent experiments were repeated five times. Scale bars, 10 cm. **b**, Expression of *PR* genes in the *zmfbl41* transposon-insertion line. The expression levels of *ZmPR4* and *ZmPR10* were detected at 24 h.p.i. by qRT–PCR. Independent experiments were repeated five times. **c**, Susceptible phenotype of rice plants overexpressing $ZmFBL41^{B73}$. Inoculated leaf sheaths of three $ZmFBL41^{B73}$-overexpressing (OE) lines are shown. Lesion length was measured in 10 plants of each line at 7 d.p.i. Independent experiments were repeated three times. Scale bars, 4 cm. **d**, Expression of *PR* genes in $ZmFBL41^{B73}$ -overexpression lines. Expression levels of *OsPR1*, *OsPR5* and *OsPR10* were detected in three $ZmFBL41^{B73}$-overexpressing lines at 24 h.p.i. by qRT–PCR. Independent experiments were repeated five times. CK indicates the expression levels at 0 h.p.i.; WT, wild type. In box plots, center values are medians and solid lines indicate variability outside the upper and lower quartiles. Statistical significance was determined using a Student's two-sided *t*-test.

resource; this line carried a *Mutator* insertion (mu1065184) in the first exon of *ZmCAD* (Supplementary Fig. 6a,b). The *zmcad* line was inoculated with *R. solani* along with the W22 line in the field, and the disease index was counted at 14 d.p.i. The *zmcad* line exhibited more serious disease symptoms than W22 after *R. solani* infection, and the disease index of *zmcad* was increased approximately 29% compared to that of W22 (Fig. 5a). Moreover, the expression of *ZmPR4* and *ZmPR10* was significantly inhibited in *zmcad* plants during *R. solani* infection (Fig. 5b).

To further validate the involvement of the *CAD* gene in BLSB resistance, we used CRISPR–Cas9 technology to knock out the *ZmCAD* homologous gene *OsCAD8B* (*LOC_Os09g23540*, *OsCAD8B* knockout) in the rice cultivar Zhonghua 11. We selected a 20-nt sequence in the *OsCAD8B* gene as a target site for Cas9 cleavage (Supplementary Fig. 6c), generated multiple putative transgenic lines and sequenced the target regions after PCR amplification. We found two mutant lines for *OsCAD8B* knockout; the *OsCAD8B* knockout genes carried a one-base-pair deletion in the target site (Supplementary Fig. 6d). The *OsCAD8B* knockout seedlings were significantly shorter than wild-type seedlings (Supplementary Fig. 6e) and the lignin content in *OsCAD8B* knockout plants (135.13 ± 5.6 mg lignin per g dry cell wall) was reduced by 26.9% compared to that in the wild-type plants (184.64 ± 17.8 mg lignin per g dry cell wall; Supplementary Fig. 6f). Furthermore, 15 annotated *CAD* genes in rice (Supplementary Table 5) suggested that there may be functional redundancy among these genes. *OsCAD8B* knockout plants were inoculated with *R. solani* for 7 d and developed longer lesions than those of Zhonghua 11 plants; the lesion length of the *OsCAD8B* knockout line was increased by approximately 3.4 cm (Fig. 5c). These results indicate that *ZmCAD* and *OsCAD* function as positive regulators in BLSB resistance.

Lignin is involved in the response of maize to *R. solani* infection. CAD is the final enzyme in the monolignol biosynthetic pathway[40]. To assess the involvement of lignin in the response of maize to *R. solani*, we measured lignin content in 12 SH lines and 10 RH lines after inoculation with *R. solani* using the acetyl bromide method[41]. Within 48 h post-inoculation (h.p.i.) with *R. solani*, lignin content first increased and later decreased in both SH and RH lines. However, the lignin content showed a tendency to be higher in the RH lines than in the SH lines, with a significant difference at 24 and 48 h.p.i. (Fig. 5d and Supplementary Table 6). Furthermore, we measured the lignin content in the *zmfbl41* and *zmcad* lines. The wild-type W22 line contained 103.1 ± 0.66 mg lignin per g dry cell wall, whereas the *zmfbl41* line contained higher levels of lignin (113.1 ± 1.62 mg lignin per g dry cell wall) and the *zmcad* line contained lower amounts of lignin (65.9 ± 2.65 mg lignin per g dry cell wall; Fig. 5e). Knocking out *ZmCAD* did not completely abolish synthesis of lignin in maize. We found that there were 12 annotated *CAD* genes in maize (Supplementary Table 5), suggesting that there is functional redundancy among these genes. These results are consistent with the well-established model in which lignin can contribute to pathogen resistance.

Natural variation in ZmFBL41 blocks the interaction with ZmCAD. Because the Chang7-2 line contains more lignin than

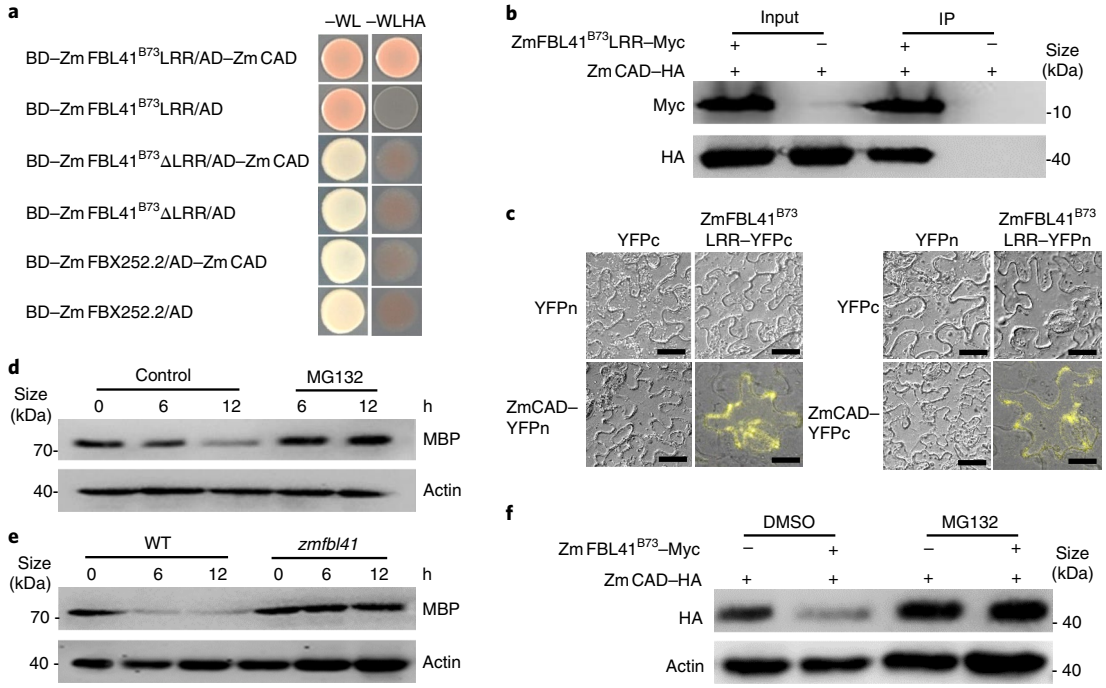

Fig. 4 | ZmFBL41^{B73} targets and triggers degradation of ZmCAD. a, Y2H assay indicates that the LRR domain of ZmFBL41^{B73} interacts with ZmCAD. ZmFBL41^{B73}ΔLRR and ZmFBX252.2 were used as controls. −WL, medium lacking Trp and Leu, −WLHA, medium lacking Trp, Leu, His and adenine. BD, pGBKT7 vector; AD, pGADT7 AD vector. Images are representative of three independent experiments. **b**, ZmFBL41^{B73}LRR interacts with ZmCAD in a co-immunoprecipitation assay. ZmFBL41^{B73}LRR–Myc and ZmCAD–HA were co-expressed in *N. benthamiana* leaves. Co-immunoprecipitation was carried out with anti-Myc and subsequently analyzed using western blotting with the anti-HA (for ZmCAD) and anti-Myc (for ZmFBL41^{B73}LRR) antibodies (see Supplementary Fig. 8a). **c**, BiFC assay shows the ZmFBL41^{B73}LRR–ZmCAD interaction in *N. benthamiana* leaf cells. Scale bars, 50 μm. Images are representative of three independent experiments. **d**, Cell-free degradation assay showed the 26S proteasome-dependent degradation of ZmCAD. MG132 (50 μM) treatment delayed ZmCAD–MBP degradation in B73 extract as revealed by western blotting with the anti-MBP antibody (see Supplementary Fig. 8b). **e**, The assay showed the delayed degradation of ZmCAD in *zmfbl41* extract by western blotting with the anti-MBP antibody (see Supplementary Fig. 8c). **f**, MG132 treatment stabilizes ZmCAD and inhibits ZmFBL41^{B73}-induced ZmCAD degradation. The ZmFBL41^{B73}–Myc and ZmCAD–HA proteins were co-expressed in *N. benthamiana* leaves, and the accumulation of ZmCAD-HA after treatment with DMSO or MG132 (50 μM) at 62 h.p.i. was analyzed by western blotting with the anti-HA antibody (see Supplementary Fig. 8d). Actin served as a loading control (**d**–**f**). Blots are representative of three independent experiments (**b**, **d**–**f**).

the B73 line, and this characteristic is associated with BLSB resistance, we assumed that the interaction between ZmCAD and the LRR domain of ZmFBL41$^{Chang7\text{-}2}$ might be inhibited. Among the four SNPs showing strong LD with the lead SNP 2867, three SNPs (SNP 2654A>G, SNP 2655G>A and SNP 2662A>C) were located in the LRR domain of *ZmFBL41* (Supplementary Fig. 7a). In comparison to the ZmFBL41^{B73}LRR domain, SNP 2654 and SNP 2655 resulted in substitution of Glu to Gly, and SNP 2662 resulted in substitution of Ser to Arg in ZmFBL41$^{Chang7\text{-}2}$ (Supplementary Fig. 7b). To assess whether the substitutions of these two amino acids affected the interaction between ZmCAD and ZmFBL41$^{Chang7\text{-}2}$LRR, we constructed point mutants of ZmFBL41^{B73}LRR (ZmFBL41^{B73}LRR(E214G), ZmFBL41^{B73}LRR(S217R) and ZmFBL41^{B73}LRR(E214G/S217R)). The interactions between these variations and ZmCAD were examined, along with those of ZmFBL41$^{Chang7\text{-}2}$LRR, by a Y2H assay. We found that ZmFBL41^{B73}LRR(E214G) and ZmFBL41^{B73}LRR(S217R) still interacted with ZmCAD, whereas ZmFBL41^{B73}LRR(E214G/S217R) and ZmFBL41$^{Chang7\text{-}2}$LRR did not interact with ZmCAD (Fig. 6a). These results demonstrate that the E214 and S217 mutations in the LRR domain interrupt the interaction of ZmFBL41$^{Chang7\text{-}2}$ with ZmCAD.

To validate the conclusion that the stability of ZmCAD is mediated by ZmFBL41$^{Chang7\text{-}2}$, we examined the degradation of ZmCAD in maize cell extracts. As shown in Fig. 6b, the accumulation of ZmCAD was significantly reduced in B73 cell extracts, whereas no reduction in ZmCAD accumulation was observed in Chang7-2 cell extracts. Furthermore, we carried out a degradation assay using a transient expression system in *N. benthamiana*. A reduction in ZmCAD accumulation induced by *ZmFBL41*^{B73} overexpression was observed, whereas ZmCAD remained stable when *ZmFBL41*$^{Chang7\text{-}2}$ was overexpressed (Fig. 6c). Additionally, we detected the degradation of ZmCAD mediated by the single point mutations in ZmFBL41^{B73} using a transient expression system in *N. benthamiana*. The results showed that a single substitution of either Glu to Gly or Ser to Arg did not affect ZmCAD degradation (Fig. 6d). Together, these results indicate that ZmFBL41$^{Chang7\text{-}2}$ could not interact with ZmCAD to promote its degradation owing to the E214 and S217 mutations in the LRR domain.

Discussion

The enrichment of plant cell walls in secondary metabolites, such as lignin, is the first layer of plant immunity, which comprises a physical barrier and elicits PAMP- and DAMP-triggered immunity[42,43]. Our results demonstrate that lignin content is increased at the beginning of infection in both SH and RH maize lines (Fig. 5d and Supplementary Table 6), consistent with a defense-related lignin accumulation response. *R. solani* is a typical necrotrophic fungus that can secrete large amounts of cell-wall-degrading enzymes (CWDEs) to destroy the plant cell wall and kill the cells at 12 h after successful colonization. Remarkably, compared with the RH lines, the increase in lignin content is markedly repressed at 24 and 48 h.p.i. in SH lines (Fig. 5d and Supplementary Table 6),

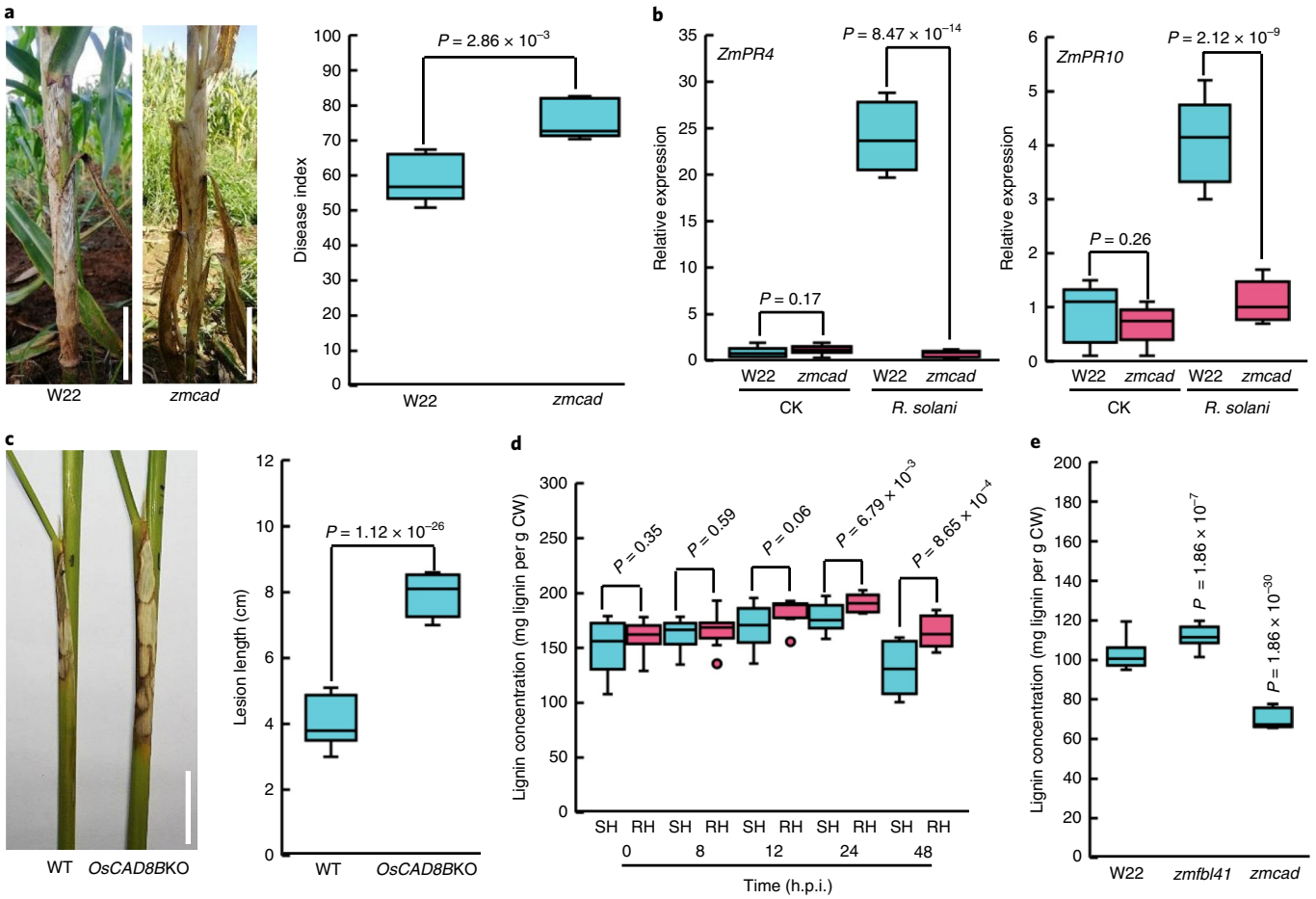

Fig. 5 | Function of *CAD* in *R. solani* resistance. a, Susceptible phenotype of the *zmcad* transposon-insertion line. An inoculated *zmcad* transposon-insertion line in the field is shown. Disease index was determined in 10 plants of each line at 14 d.p.i. Independent experiments were repeated five times. Scale bars, 10 cm. **b**, Expression of *PR* genes in the *zmcad* insertion line. The expression levels of *ZmPR4* and *ZmPR10* were detected at 24 h.p.i. by qRT–PCR. Independent experiments were repeated five times. **c**, Susceptible phenotype of the *OsCAD8B* knockout transgenic line. An inoculated leaf sheath of the *OsCAD8B* knockout line is shown. Lesion length was measured at 7 d.p.i. in 10 plants of each line. Independent experiments were repeated three times. Scale bars, 2 cm. **d**, Lignin analysis of 12 SH lines and 10 RH lines inoculated with *R. solani* for 48 h. CW, cell wall. **e**, Determination of lignin content in *zmfbl41* and *zmcad* transposon-insertion lines. Ten single plants of each line were measured. Independent experiments were repeated three times. In box plots, center values are medians, solid lines indicate variability outside the upper and lower quartiles and dots denote outliers. Statistical significance was determined using a Student's two-sided *t*-test.

suggesting that utilizing a host F-box protein to interfere with lignin synthesis has a critical role in the response to *R. solani* infection by breaking the physical barriers and blocking the cell wall apposition-mediated defense. Therefore, we present a model to summarize our hypothesis (Fig. 7). In susceptible maize lines, ZmCAD is recruited by ZmFBL41 and degraded by the 26S proteasome during the early infection process. The degradation of ZmCAD interferes with lignin synthesis and reduces the strength of the plant cell wall, which benefits fungal colonization. Lines resistant to *R. solani*, such as Chang7-2, have evolved the *ZmFBL41*$^{Chang7\text{-}2}$ allele by mutation to evade its interaction with and degradation of ZmCAD (Fig. 7). Thus, we have uncovered a molecular mechanism by which *R. solani* suppresses maize immunity and a mechanism that maize has evolved to fight against infection by *R. solani*.

The plant cell wall provides a mechanical barrier against pathogens, and alterations in the cell wall have been demonstrated to have considerable effects on disease resistance[43–47]. To colonize plant tissues, pathogens have evolved weapons to penetrate and break down this barrier, such as CWDEs and appressoria[48–50]. During the early stage of *R. solani* infection, *R. solani* secretes multiple CWDEs, including polygalacturonase, polymethyl-galacturonase, cellulase and β-glucosidase, to facilitate its invasion[51,52]. Lignin is a major component of the cell wall and has a crucial role in plant growth and development, in addition to the innate immune response of the plant to biotic stresses[41,53–55]. In this study, lignin content increased within 24 h.p.i. with *R. solani* (Fig. 5d and Supplementary Table 6), consistent with the activation of lignin synthesis as one of the components of basal immunity through the protection of cell wall integrity. More importantly, the failure of the interaction between ZmFBL41 and ZmCAD maintains the accumulation of lignin and resistance to *R. solani* (Figs. 4, 5), suggesting that suppressing host lignin synthesis is required for *R. solani* infection. Recently, the *Arabidopsis* polygalacturonase gene *ADPG2* was found to be induced by *Pseudomonas syringae* pv. tomato DC3000 to enhance susceptibility[56]. We found that *R. solani* could manipulate the maize SCF^{ZmFBL41} E3 ligase complex to destroy maize cell wall integrity during its infection, in addition to using its own CWDEs. These results reveal a previously undescribed virulence mechanism in this phytopathogen. Furthermore, some of the other plant secondary chemicals downstream of CAD may also be altered due to the degradation of CAD, and may also be partially responsible for the BLSB resistance.

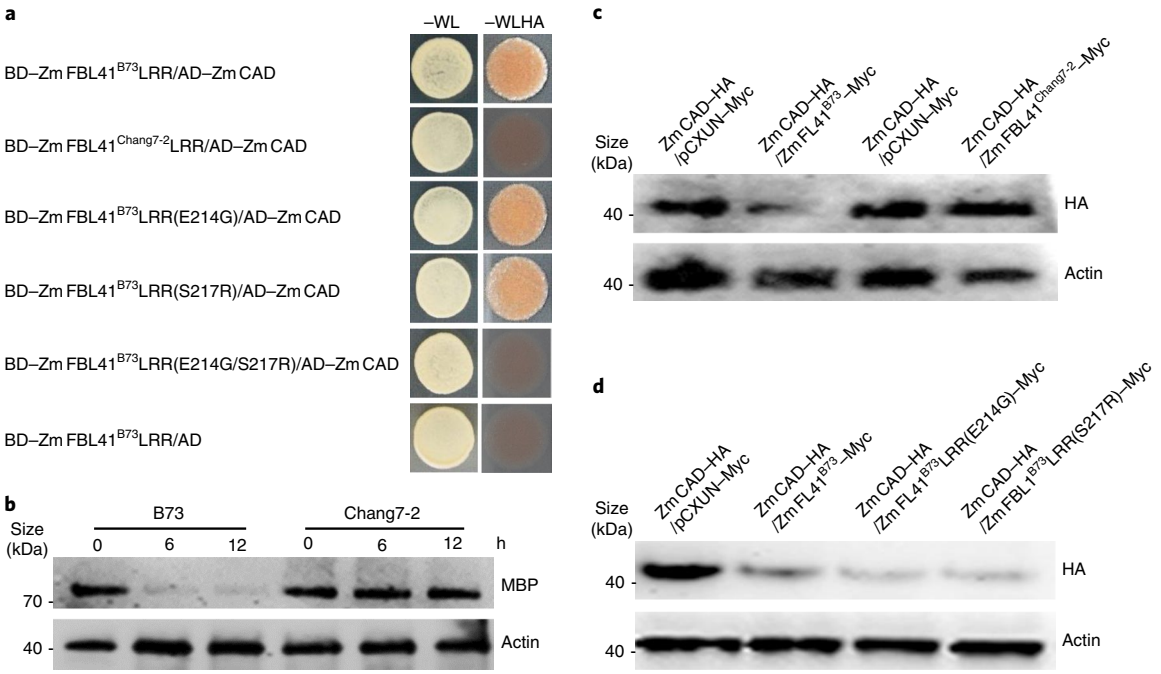

Fig. 6 | Two amino acid substitutions in the LRR domain of ZmFBL41$^{Chang7-2}$ stabilize ZmCAD by blocking protein–protein interactions. a, The Y2H assay indicated that substitutions of Glu to Gly and Ser to Arg in the LRR domain result in the loss of the interaction between ZmFBL41$^{Chang7-2}$ and ZmCAD. –WL, medium lacking Trp and Leu; –WLHA, medium lacking Trp, Leu, His and adenine. Images are representative of three independent experiments. **b**, Cell-free degradation assay showed the stabilization of ZmCAD in Chang7-2 extract (see Supplementary Fig. 8e). **c**, The transient expression assay in *N. benthamiana* showed that ZmFBL41$^{Chang7-2}$ failed to trigger degradation of ZmCAD. The ZmCAD–HA and ZmFBL41^{B73}–Myc or ZmFBL41$^{Chang7-2}$–Myc proteins were co-expressed in *N. benthamiana* leaves, and the accumulation of ZmCAD was analyzed by western blotting with the anti-HA (for ZmCAD) antibody (see Supplementary Fig. 8f). **d**, The transient expression assay in *N. benthamiana* showed that the substitution of Glu to Gly or Ser to Arg in ZmFBL41^{B73} did not affect the degradation of ZmCAD. The ZmCAD–HA and ZmFBL41^{B73}–Myc, ZmFBL41^{B73}LRR(E214G)–Myc or ZmFBL41^{B73}LRR(S217R)–Myc proteins were co-expressed in *N. benthamiana* leaves, and the accumulation of ZmCAD was analyzed by western blotting with the anti-HA (for ZmCAD) antibody (see Supplementary Fig. 8g). Actin served as a loading control and blots are representative of three independent experiments (**b**–**d**).

The F-box protein family is large, functionally diverse and distributed across all eukaryotes; these proteins have important roles in almost all aspects of growth and development, as well as in responses to biotic and abiotic stress in plants[57,58]. Many F-box proteins have been shown to be involved in plant immune responses. In *Arabidopsis*, the F-box protein COI1 acts as a positive regulator in jasmonate signaling[59]. The F-box protein MAX2, a positive regulator of PTI, contributes to resistance to bacterial phytopathogens[60]. By contrast, the F-box proteins CPR1, CPR30 and SON1 are negative regulators of innate immunity[61–63]. In rice, overexpressing the F-box protein gene *OsDRF1* could improve disease resistance[64]. Therefore, many F-box proteins in plants may function as either negative or positive regulators in innate immunity, depending on their substrate specificity. There are over 300 F-box proteins in maize, and most of them still lack functional characterization[65]. In this study, we identified the BLSB quantitative resistance gene *ZmFBL41* in maize by GWAS (Fig. 1). *ZmFBL41*^{B73} overexpression results in susceptibility to *R. solani*, and knockout of *ZmFBL41* results in enhanced resistance (Fig. 3), indicating that *ZmFBL41*^{B73} functions as a negative regulator in BLSB resistance. We show that natural variation in an F-box protein considerably contributes to BLSB resistance in maize. Our results demonstrate that ZmFBL41^{B73} interacts with ZmCAD and promotes ZmCAD degradation by the 26S proteasome (Fig. 4). Given the evidence, this F-box protein could target secondary metabolism to regulate plant defense.

Some pathogen effectors have evolved the ability to interfere with the host E3 ligase complex to promote disease[30]. For example, the AvrPiz-t effector of the rice blast fungus *Magnaporthe oryzae* inhibits the E3 ligase activity of APIP6, resulting in suppression of the PAMP-induced production of reactive oxygen species and susceptibility to *M. oryzae*[66]. The Avr3a effector from *Phytophthora infestans* targets the E3 ligase CMPG1 to suppress INF1-triggered cell death[67–69]. However, the regulatory mechanism of ZmFBL41 remains unclear. Because the expression of *ZmFBL41* is similar in susceptible and resistant maize lines (Fig. 2c), *R. solani* may deliver effectors to directly or indirectly interact with ZmFBL41 or ZmSKP1-1; this mechanism should be further explored.

BLSB is a soil-borne disease caused by the necrotrophic fungus *R. solani*, which is more prevalent in humid weather and can survive for several years in the soil. After a marked increase owing to condensed planting technology and straw-returning methods, BLSB is becoming a more severe disease, resulting in yield reductions ranging from 10% to 40% in maize. In addition, *R. solani* has a wide range of alternative hosts, infecting many members of the Poaceae, Fabaceae and Solanaceae families. In China, sheath blight is the disease with the highest incidence in rice and wheat. Genetic resistance is a key component of disease management. In this study, two amino acid substitutions in ZmFBL41 determine a *R. solani*-resistant phenotype, suggesting that *zmfbl41* is a recessive gene responsible for BLSB resistance in maize. This locus is the first cloned BLSB-related QTL and it therefore represents a crucial target for developing *R. solani* resistance through maize breeding. The advent of CRISPR–Cas9, which allows researchers to engineer the genome precisely even at the single-base level, has enabled the development of genetic resistance in crops[70–72]. Thus, the corresponding dominant allele of the recessive resistance gene *fbl41* could be edited by CRISPR–Cas9 to convert it to a resistant variety in rice and other plant species in the future.

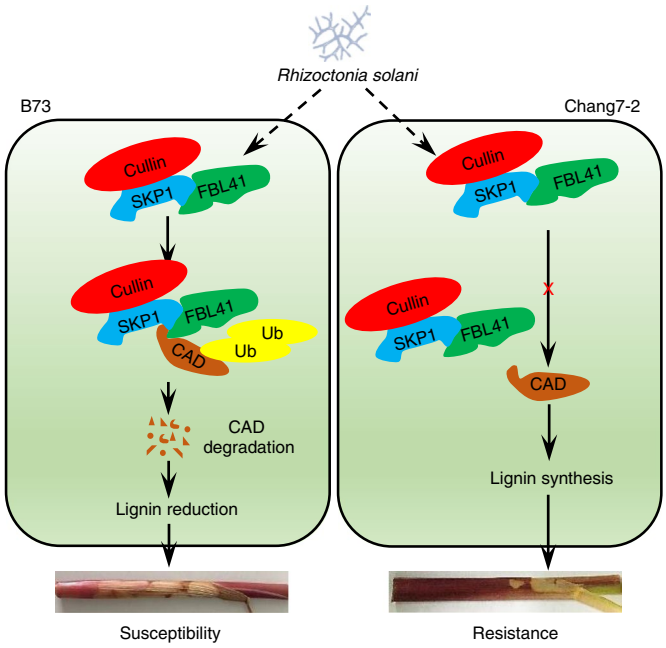

Fig. 7 | A model for ZmFBL41-mediated BLSB resistance. In B73, FBL41 interacts with SKP1 to form the SCF^{FBL41} complex, and recruits CAD for 26S proteasome-mediated degradation, resulting in reduced lignin synthesis and increased susceptibility to *R. solani*. In resistant maize lines, such as Chang7-2, FBL41 fails to recruit CAD for degradation, leading to the accumulation of lignin and increased resistance to *R. solani*.

Online content

Any methods, additional references, Nature Research reporting summaries, source data, statements of code and data availability and associated accession codes are available at https://doi.org/10.1038/s41588-019-0503-y.

Received: 4 November 2018; Accepted: 19 August 2019;
Published online: 30 September 2019

References

1. Wen, W., Brotman, Y., Willmitzer, L., Yan, J. & Fernie, A. R. Broadening our portfolio in the genetic improvement of maize chemical composition. *Trends Genet.* **32**, 459–469 (2016).
2. Lu, G. et al. Quantitative trait loci mapping of maize yield and its components under different water treatments at flowering time. *J. Integr. Plant Biol.* **48**, 1233–1243 (2006).
3. Xiao, Y., Liu, H., Wu, L., Warburton, M. & Yan, J. Genome-wide association studies in maize: praise and stargaze. *Mol. Plant* **10**, 359–374 (2017).
4. Flint-Garcia, S., Thornsberry, J. & Buckler, E. Structure of linkage disequilibrium in plants. *Annu. Rev. Plant Biol.* **54**, 357–374 (2003).
5. Risch, N. & Merikangas, K. The future of genetic studies of complex human diseases. *Science* **273**, 1516–1517 (1996).
6. Visscher, P. M., Brown, M. A., McCarthy, M. I. & Yang, J. Five years of GWAS discovery. *Am. J. Hum. Genet.* **90**, 7–24 (2012).
7. Tian, F. et al. Genome-wide association study of leaf architecture in the maize nested association mapping population. *Nat. Genet.* **43**, 159–162 (2011).
8. Li, H. et al. Genome-wide association study dissects the genetic architecture of oil biosynthesis in maize kernels. *Nat. Genet.* **45**, 43–50 (2013).
9. Si, L. et al. *OsSPL13* controls grain size in cultivated rice. *Nat. Genet.* **48**, 447–456 (2016).
10. Wang, X. et al. Genetic variation in *ZmVPP1* contributes to drought tolerance in maize seedlings. *Nat. Genet.* **48**, 1233–1241 (2016).
11. Yano, K. et al. Genome-wide association study using whole-genome sequencing rapidly identifies new genes influencing agronomic traits in rice. *Nat. Genet.* **48**, 927–934 (2016).
12. Li, W. et al. A natural allele of a transcription factor in rice confers broad-spectrum blast resistance. *Cell* **170**, 114–126 (2017).
13. Ding, J. et al. Genome-wide association mapping reveals novel sources of resistance to northern corn leaf blight in maize. *BMC Plant Biol.* **15**, 206 (2015).
14. Gowda, M. et al. Genome-wide association and genomic prediction of resistance to maize lethal necrosis disease in tropical maize germplasm. *Theor. Appl. Genet.* **128**, 1957–1968 (2015).
15. Mammadov, J. et al. Combining powers of linkage and association mapping for precise dissection of QTL controlling resistance to gray leaf spot disease in maize (*Zea mays* L.). *BMC Genom.* **16**, 916 (2015).
16. Tang, J. D., Perkins, A., Williams, W. P. & Warburton, M. L. Using genome-wide associations to identify metabolic pathways involved in maize aflatoxin accumulation resistance. *BMC Genom.* **16**, 673 (2015).
17. Mahuku, G. et al. Combined linkage and association mapping identifies a major QTL (*qRtsc8-1*), conferring tar spot complex resistance in maize. *Theor. Appl. Genet.* **129**, 1217–1229 (2016).
18. Zhao, M. et al. Quantitative trait loci for resistance to banded leaf and sheath blight in maize. *Crop Sci.* **46**, 1039–1045 (2006).
19. Zheng, A. et al. The evolution and pathogenic mechanisms of the rice sheath blight pathogen. *Nat. Commun.* **4**, 1424 (2013).
20. Sha, X. Y. & Zhu, L. H. Resistance of some rice varieties to sheath blight (ShB). *Int. Rice Res. Newslett.* **15**, 7–8 (1989).
21. Li, Z., Pinson, S. R. M., Marchetti, M. A., Stansel, J. W. & Park, W. D. Characterization of quantitative trait loci (QTLs) in cultivated rice contributing to field resistance to sheath blight (*Rhizoctonia solani*). *Theor. Appl. Genet.* **91**, 382–388 (1995).
22. Channamallikarjuna, V. et al. Identification of major quantitative trait loci *qSBR11-1* for sheath blight resistance in rice. *Mol. Breed.* **25**, 155–166 (2010).
23. Wang, Y., Pinson, S. R. M., Fjellstrom, R. G. & Tabien, R. E. Phenotypic gain from introgression of two QTL, *qSB9-2* and *qSB12-1*, for rice sheath blight resistance. *Mol. Breed.* **30**, 293–303 (2012).
24. Wang, H. et al. Rice WRKY4 acts as a transcriptional activator mediating defense responses toward *Rhizoctonia solani*, the causing agent of rice sheath blight. *Plant Mol. Biol.* **89**, 157–171 (2015).
25. Richa, K. et al. Novel chitinase gene *LOC_Os11g47510* from Indica rice Tetep provides enhanced resistance against sheath blight pathogen *Rhizoctonia solani* in rice. *Front. Plant Sci.* **8**, 596 (2017).
26. Li, N. et al. OsASR2 regulates the expression of a defence-related gene, *Os2H16*, by targeting the GT-1 *cis*-element. *Plant Biotechnol. J.* **16**, 771–783 (2018).
27. Furlan, G. et al. Changes in PUB22 ubiquitination modes triggered by MITOGEN-ACTIVATED PROTEIN KINASE3 dampen the immune response. *Plant Cell* **29**, 726–745 (2017).
28. Tong, M. et al. E3 ligase SAUL1 serves as a positive regulator of PAMP-triggered immunity and its homeostasis is monitored by immune receptor SOC3. *New Phytol.* **215**, 1516–1532 (2017).
29. Hammoudi, V. et al. The *Arabidopsis* SUMO E3 ligase SIZ1 mediates the temperature dependent trade-off between plant immunity and growth. *PLoS Genet.* **14**, e1007157 (2018).
30. Duplan, V. & Rivas, S. E3 ubiquitin-ligases and their target proteins during the regulation of plant innate immunity. *Front. Plant Sci.* **5**, 42 (2014).
31. Wang, J. et al. Overexpression of *VpEIFP1*, a novel F-box/Kelch-repeat protein from wild Chinese *Vitis pseudoreticulata*, confers higher tolerance to powdery mildew by inducing thioredoxin z proteolysis. *Plant Sci.* **263**, 142–155 (2017).
32. Huang, J., Zhu, C. & Li, X. $SCF^{SNIPER4}$ controls the turnover of two redundant TRAF proteins in plant immunity. *Plant J.* **95**, 504–515 (2018).
33. Yang, X. et al. Characterization of a global germplasm collection and its potential utilization for analysis of complex quantitative traits in maize. *Mol. Breed.* **28**, 511–526 (2011).
34. Fu, J. et al. RNA sequencing reveals the complex regulatory network in the maize kernel. *Nat. Commun.* **4**, 2832 (2013).
35. Jain, M. et al. F-Box proteins in rice. Genome-wide analysis, classification, temporal and spatial gene expression during panicle and seed development, and regulation by light and abiotic stress. *Plant Physiol.* **143**, 1467–1483 (2007).
36. Kipreos, E. T. & Pagano, M. The F-box protein family. *Genom. Biol.* **1**, reviews3002.1 (2000).
37. Zheng, N. et al. Structure of the Cul1–Rbx1–Skp1–F box^{Skp2} SCF ubiquitin ligase complex. *Nature* **416**, 703–709 (2002).
38. Skaar, J. R., Pagan, J. K. & Pagano, M. Mechanisms and function of substrate recruitment by F-box proteins. *Nat. Rev. Mol. Cell Biol.* **14**, 369–381 (2013).
39. Xu, C. et al. Degradation of MONOCULM 1 by APC/C^{TAD1} regulates rice tillering. *Nat. Commun.* **3**, 750 (2012).
40. Jun, S. Y. et al. The enzyme activity and substrate specificity of two major cinnamyl alcohol dehydrogenases in sorghum (*Sorghum bicolor*), SbCAD2 and SbCAD4. *Plant Physiol.* **174**, 2128–2145 (2017).
41. Chezem, W. R., Memon, A., Li, F., Weng, J. & Clay, N. K. SG2-type R2R3-MYB transcription factor MYB15 controls defense-induced lignification and basal immunity in *Arabidopsis*. *Plant Cell* **29**, 1907–1926 (2017).
42. Underwood, W. The plant cell wall: a dynamic barrier against pathogen invasion. *Front. Plant Sci.* **3**, 85 (2012).
43. Malinovsky, F. G., Fangel, J. U. & Willats, W. G. The role of the cell wall in plant immunity. *Front. Plant Sci.* **5**, 178 (2014).

44. Bellincampi, D., Cervone, F. & Lionetti, V. Plant cell wall dynamics and wall-related susceptibility in plant-pathogen interactions. *Front. Plant Sci.* **5**, 228 (2014).
45. Escudero, V. et al. Alteration of cell wall xylan acetylation triggers defense responses that counterbalance the immune deficiencies of plants impaired in the β-subunit of the heterotrimeric G-protein. *Plant J.* **92**, 386–399 (2017).
46. Lionetti, V. et al. Three pectin methylesterase inhibitors protect cell wall integrity for *Arabidopsis* immunity to *Botrytis*. *Plant Physiol.* **173**, 1844–1863 (2017).
47. Bacete, L., Melida, H., Miedes, E. & Molina, A. Plant cell wall-mediated immunity: cell wall changes trigger disease resistance responses. *Plant J.* **93**, 614–636 (2018).
48. Kubicek, C. P., Starr, T. L. & Glass, N. L. Plant cell wall-degrading enzymes and their secretion in plant-pathogenic fungi. *Annu. Rev. Phytopathol.* **52**, 427–451 (2014).
49. Paccanaro, M. C. et al. Synergistic effect of different plant cell wall-degrading enzymes is important for virulence of *Fusarium graminearum*. *Mol. Plant Microbe Interact.* **30**, 886–895 (2017).
50. Zhu, X. et al. Silencing *PsKPP4*, a MAP kinase kinase kinase gene, reduces pathogenicity of the stripe rust fungus. *Mol. Plant Pathol.* **19**, 2590–2602 (2018).
51. Lakshman, D. K. et al. Proteomic investigation of *Rhizoctonia solani* AG4 identifies secretome and mycelial proteins with roles in plant cell wall degradation and virulence. *J. Agric. Food Chem.* **64**, 3101–3110 (2016).
52. Wibberg, D. et al. Genome analysis of the sugar beet pathogen *Rhizoctonia solani* AG2-2IIIB revealed high numbers in secreted proteins and cell wall degrading enzymes. *BMC Genom.* **17**, 245 (2016).
53. Boerjan, W., Ralph, J. & Baucher, M. Lignin biosynthesis. *Annu. Rev. Plant Biol.* **54**, 519–546 (2003).
54. Weng, J. K. & Chapple, C. The origin and evolution of lignin biosynthesis. *New Phytol.* **187**, 273–285 (2010).
55. Ma, Q., Zhu, H. & Qiao, M. Contribution of both lignin content and sinapyl monomer to disease resistance in tobacco. *Plant Pathol.* **67**, 642–650 (2018).
56. Wang, X. et al. IDL6-HAE/HSL2 impacts pectin degradation and resistance to *Pseudomonas syringae* pv tomato DC3000 in *Arabidopsis* leaves. *Plant J.* **89**, 250–263 (2017).
57. Lechner, E., Achard, P., Vansiri, A., Potuschak, T. & Genschik, P. F-box proteins everywhere. *Curr. Opin. Plant Biol.* **9**, 631–638 (2006).
58. Somers, D. E. & Fujiwara, S. Thinking outside the F-box: novel ligands for novel receptors. *Trends Plant Sci.* **14**, 206–213 (2009).
59. Thines, B. et al. JAZ repressor proteins are targets of the SCF^{COI1} complex during jasmonate signaling. *Nature* **448**, 661–665 (2007).
60. Piisilä, M. et al. The F-box protein MAX2 contributes to resistance to bacterial phytopathogens in *Arabidopsis thaliana*. *BMC Plant Biol.* **15**, 53 (2015).
61. Gou, M. et al. The F-box protein CPR1/CPR30 negatively regulates R protein SNC1 accumulation. *Plant J.* **69**, 411–420 (2012).
62. Gou, M. et al. An F-box gene, *CPR30*, functions as a negative regulator of the defense response in *Arabidopsis*. *Plant J.* **60**, 757–770 (2009).
63. Kim, H. S. & Delaney, T. P. *Arabidopsis* SON1 is an F-box protein that regulates a novel induced defense response independent of both salicylic acid and systemic acquired resistance. *Plant Cell* **14**, 1469–1482 (2002).
64. Cao, Y. et al. Overexpression of a rice defense-related F-box protein gene *OsDRF1* in tobacco improves disease resistance through potentiation of defense gene expression. *Physiol. Plant.* **134**, 440–452 (2008).
65. Jia, F., Wu, B., Li, H., Huang, J. & Zheng, C. Genome-wide identification and characterization of F-box family in maize. *Mol. Genet. Genom.* **288**, 559–577 (2013).
66. Park, C. H. et al. The *Magnaporthe oryzae* effector AvrPiz-t targets the RING E3 ubiquitin ligase APIP6 to suppress pathogen-associated molecular pattern-triggered immunity in rice. *Plant Cell* **24**, 4748–4762 (2012).
67. Gonzalez-Lamothe, R. et al. The U-box protein CMPG1 is required for efficient activation of defense mechanisms triggered by multiple resistance genes in tobacco and tomato. *Plant Cell* **18**, 1067–1083 (2006).
68. Bos, J. I. et al. *Phytophthora infestans* effector AVR3a is essential for virulence and manipulates plant immunity by stabilizing host E3 ligase CMPG1. *Proc. Natl Acad. Sci. USA* **107**, 9909–9914 (2010).
69. Gilroy, E. M. et al. CMPG1-dependent cell death follows perception of diverse pathogen elicitors at the host plasma membrane and is suppressed by *Phytophthora infestans* RXLR effector AVR3a. *New Phytol.* **190**, 653–666 (2011).
70. Chandrasekaran, J. et al. Development of broad virus resistance in non-transgenic cucumber using CRISPR/Cas9 technology. *Mol. Plant Pathol.* **17**, 1140–1153 (2016).
71. Jia, H. et al. Genome editing of the disease susceptibility gene *CsLOB1* in citrus confers resistance to citrus canker. *Plant Biotechnol. J.* **15**, 817–823 (2017).
72. Zhang, Y. et al. Simultaneous modification of three homoeologs of *TaEDR1* by genome editing enhances powdery mildew resistance in wheat. *Plant J.* **91**, 714–724 (2017).

Acknowledgements

We thank B. Liu and Y. Zhang from Shandong Agricultural University for seed propagation of maize transposon-insertion lines. This study was supported by the National Key Research and Development Program of China (2016YFD0101003 and 2016YFD0100903), the National Natural Science Foundation of China (31601279), the Key Research and Development Program of Shandong Province (2017GNC10104 and 2018GNC110018) and the Shandong Modern Agricultural Technology and Industry system (SDAIT-17-06).

Author contributions

N.L. inoculated the maize population, resequenced *ZmFBL41*, carried out the functional analysis of *ZmFBL41* and *ZmCAD*, screened ZmFBL41-interacting proteins, carried out the expression analysis of *ZmFBL41* and *PR* genes, measured the lignin content and wrote the paper. B.L. studied the degradation of ZmCAD and measured the lignin content. H.W. analyzed the GWAS data. X.L. inoculated the maize population. F.Y. studied the degradation of ZmCAD and constructed the *OsCAD8B* knockout line. X.D. analyzed the raw data. J.Y. provided the maize inbred lines and SNP data platform. Z.C. designed the experiments and wrote the paper.

Competing interests

The authors declare no competing interests.

Additional information

Supplementary information is available for this paper at https://doi.org/10.1038/s41588-019-0503-y.

Correspondence and requests for materials should be addressed to Z.C.

Reprints and permissions information is available at www.nature.com/reprints.

Publisher's note Springer Nature remains neutral with regard to jurisdictional claims in published maps and institutional affiliations.

Methods

Phenotyping of maize BLSB resistance and GWAS. Phenotyping of BLSB resistance was performed in an association-mapping panel composed of 318 maize inbred lines[33]. For each line, 10 plants were randomly grown in the field and the third sheath from the ground was inoculated with *R. solani* for 5 d. The length of each lesion was measured and the mean was calculated. GWAS was performed in TASSEL v.3.0 (ref. [73]) using high-quality data for the 542,438 SNPs[8,34] with minor allele frequency of ≥0.05. The GLM approach controlling population structure (Q) was adopted after comparing the performances of four linear models, that is, GLM, GLM + Q, GLM + K and GLM + Q + K, using Structure 2.3.4 software. The compromised significance threshold for GWAS was set as $P < 1 \times 10^{-5}$ based on the Bonferroni-adjusted correction of multiple testing.

Prokaryotic expression and protein purification. The *ZmCAD* coding sequence (CDS) was cloned into the pMal-c2X vector between the EcoRI and SalI sites, and the fusion construct was transformed into BL21(DE3) *Escherichia coli*. Then, the transformed bacteria were grown at 37 °C in Luria–Bertani medium containing 100 mg ml^{-1} kanamycin to an optical density at 600 nm (OD_{600}) of 0.6. The fusion protein ZmCAD–MBP was induced by adding 1 mM isopropyl-1-thio-β-galactopyranoside and incubating at 37 °C for 6 h. ZmCAD–MBP was purified using amylose resin (New England Biolabs) following the manufacturer's instructions.

Co-immunoprecipitation. The CDSs of *ZmFBL41*^{B73}*LRR* and *ZmCAD* were cloned into the pCXUN–Myc and pCXUN–HA vectors[74], respectively. The recombinant constructs were transformed into *Agrobacterium tumefaciens* strain GV3101. Then, the *Agrobacterium* strains (containing the *ZmFBL41*^{B73}*LRR* and *ZmCAD* expression vectors) were resuspended in induction medium (10 mM MES-KOH, pH 5.7, 10 mM $MgCl_2$, 200 mM acetosyringone), mixed (final OD_{600} of each *Agrobacterium* is 0.5), and infiltrated into *N. benthamiana* leaves with *Agrobacterium* carrying p19 (35S:p19). Total protein was extracted with extraction buffer (50 mM Tris-HCl, pH 7.5, 150 mM NaCl, 50 mM sucrose, 0.1% Triton X-100, 0.5 mM dithiothreitol, 10 mM NaF, 1 mM Na_3VO_4, 25 mM glycerol phosphate, 1 mM benzylsulfonyl fluoride, 1× protease inhibitor cocktail) at 3 d.p.i. Co-immunoprecipitation was performed with Pierce anti-Myc magnetic beads (Thermo Scientific). Western blotting was performed using anti-Myc and anti-HA antibodies. Co-immunoprecipitation of ZmSKP1-1–Myc and ZmFBL41^{B73}–HA or ZmSKP1-1–Myc and ZmFBL41^{B73}ΔLRR–HA was also carried out using the same method as described above.

Subcellular localization. To determine the subcellular localization of ZmFBL41, the full-length CDS was cloned into the pEarleyGate 103 vector using Gateway BP Clonase II Enzyme Mix (Thermo Scientific). The fusion construct was transformed into *A. tumefaciens* strain GV3101, and the bacterial suspension ($OD_{600} = 0.5$) was infiltrated into *N. benthamiana* leaves with *Agrobacterium* carrying p19. *N. benthamiana* leaves transformed with p35S:GFP were used as controls. Fluorescence was examined under a two-photon laser confocal microscope (Zeiss LSM880 NLO,) 3 d after transformation.

BiFC assay. The coding regions of *ZmFBL41*^{B73}*LRR* and *ZmCAD* were cloned into the pSPYCE-35S and pSPYNE-35S vectors, respectively. Each was fused separately to the C-terminal half (*ZmFBL41*^{B73}*LRR*/*ZmCAD*–YFPc) and the N-terminal half (*ZmFBL41*^{B73}*LRR*/*ZmCAD*–YFPn) of yellow fluorescent protein (YFP); YFPc and YFPn were used alone as controls. These constructs were transformed into *A. tumefaciens* strain GV3101 and co-infiltrated into *N. benthamiana* leaves with *Agrobacterium* carrying p19. Fluorescence was examined under a two-photon laser confocal microscope (Zeiss LSM880 NLO) at 3 d after transformation. BiFC assays of ZmSKP1-1 and ZmFBL41^{B73} or ZmSKP1-1 and ZmFBL41^{B73}ΔLRR were also carried out using the same method as described above.

RNA extraction and qRT–PCR. Total RNA was extracted using TRIzol reagent (Sigma-Aldrich) according to the manufacturer's protocols. cDNA was conducted with a ReverTra Ace qPCR RT Master Mix with gDNA Remover kit (Toyobo Life Science). qRT–PCR was performed with a KOD SYBR qPCR Mix kit (Toyobo Life Science) in a qTOWER^3 Thermal Cycler (Analytik). *ZmACTIN* and *OsACTIN* were used to normalize all qRT–PCR data. The relative expression was calculated using the $2^{-\Delta\Delta C_t}$ method. The primers are listed in Supplementary Table 7.

Y2H assay. The full-length CDSs of *ZmCAD* and *ZmFBL41LRR*, *ZmFBL41ΔLRR* or *ZmFBX252.2* were cloned into the pGADT7 AD and pGBKT7 vectors, respectively. Then, the two constructs were co-transformed into Y2HGold yeast cells (Transgen Biotech). The empty vector pGADT7 AD was co-transformed as a negative control. The interaction was determined on synthetically defined (SD)/−Ade/−His/−Leu/−Trp medium following the manufacturer's protocols (Clontech). Y2H assays of ZmSKP1-1 and ZmFBL41ΔLRR or ZmFBL41ΔF-box were performed using the same method as described above.

***Rhizoctonia* solani inoculation.** *R. solani* strain YWK196 was first grown on potato–dextrose–agar medium at 25 °C for 7 d. The fungal blocks were then transformed into PDB medium containing matchsticks and grown at 25 °C until the hyphae twined around the matchsticks. The matchsticks with hyphae were inserted into plant sheaths. Lesion length was measured at 7 d.p.i. in the greenhouse, and the disease index was determined at 14 d.p.i. in the field.

Cell-free protein degradation assay. Maize total protein was extracted with degradation buffer (50 mM Tris-HCl, pH 7.5, 150 mM NaCl, 50 mM sucrose, 0.1% Triton X-100, 1 mM EDTA, 10 mM ATP, 1 mM benzylsulfonyl fluoride, 1× protease inhibitor cocktail) and adjusted to equal concentrations. To detect the degradation of ZmCAD–MBP, 100 ng purified ZmCAD–MBP protein was added into 100 µl of each maize extract. The reaction mixtures were incubated with or without 50 µM MG132 at 28 °C for the indicated times. Reactions were blocked by adding SDS–PAGE sample buffer. The samples were analyzed by western blotting using the anti-MBP antibody.

Protein degradation assay in the transient expression system in *N. benthamiana*. The CDS of *ZmFBL41* was cloned into the pCXUN–Myc vector and the construct was transformed into *A. tumefaciens* strain GV3101. The *Agrobacterium* strains containing *ZmFBL41* and *ZmCAD* were co-infiltrated into *N. benthamiana* leaves with *Agrobacterium* carrying p19. Leaves were collected at 3 d.p.i. For MG132 treatment, leaves were sprayed with 20 µM MG132 or 1% DMSO only, and leaves were collected 2 h after spraying. Total protein was extracted with extraction buffer (50 mM Tris-HCl pH 7.5, 150 mM NaCl, 50 mM sucrose, 0.1% Triton X-100, 1 mM EDTA, 1 mM benzylsulfonyl fluoride, 1× protease inhibitor cocktail) and adjusted to equal concentrations. Protein degradation was detected by western blotting using the anti-HA antibody. Protein degradation assays of ZmCAD and ZmFBL41^{B73}LRR(E214G) or ZmFBL41^{B73}LRR(S217R) were performed using the same method as described above.

Extraction and quantification of lignin. Dry samples (0.3 g) were ground in liquid nitrogen and suspended in 7 ml potassium phosphate buffer (50 mM, pH 7.0). The sample was pelleted by centrifugation (1,400*g*, 5 min) and the pellet was extracted with the following solvents for 15 min each: two times with 7 ml PBS (pH 7.0), three times with 7 mL PBS containing 1% (v/v) Triton X-100, two times with 7 ml PBS containing 1 M NaCl, two times with 7 ml distilled water and two times with 5 ml acetone. Then, the pellet was dried at 60 °C for 24 h. Subsequently, 20 mg of dry pellet was added to 0.5 ml of 25% acetyl bromide (v/v in glacial acetic acid) and incubated at 70 °C for 30 min. After quickly cooling in an ice bath, the sample was mixed with 0.9 ml of 2 M NaOH, 0.1 ml of 5 M hydroxylamine-HCl and 6 ml of glacial acetic acid for complete solubilization of the lignin extract. The absorbance of the supernatant was measured at 280 nm after centrifugation (1,400*g*, 5 min). Lignin content was calculated using the extinction coefficient 22.9 g^{-1} l cm^{-1} with Beer's law ($A = \varepsilon lc$).

Plasmid construction and rice transformation. For *ZmFBL41* overexpression, the full-length CDS of *ZmFBL41* was cloned into the pCXUN vector and introduced into the rice cultivar Zhonghua 11 through *Agrobacterium*-mediated transformation as described previously[75]. The transgenic plants were verified by PCR, and the expression level of *ZmFBL41* in transgenic plants was confirmed by qRT–PCR.

For *OsCAD8B* knockout, a 23-bp targeting sequence (including protospacer adjacent motif) was selected within the *OsCAD8B* gene, and the sequence was synthesized and annealed to form the oligonucleotide adapter. The adaptor was ligated into the pYLgRNA-OsU3 vector digested by BsaI. The gRNA expression cassette was amplified from the ligation product and purified using a gel extraction kit (Omega). Then, the purified gRNA expression cassette was ligated into the pYLCRISPR–Cas9-MH vector[76] digested by BsaI, and the ligation product was transformed into *E. coli* competent cells to produce the CRISPR–Cas9 plasmid. The CRISPR–Cas9 plasmid was introduced into the rice cultivar Zhonghua 11 through *Agrobacterium*-mediated transformation as described above. The target was amplified by PCR using primer pairs flanking the designed target site, and the PCR product was sequenced.

Statistical analysis. The statistical tests are described throughout the Article and in the figure legends. Two-tailed Student's *t*-tests were performed to compare *ZmFBL41* expression levels between SH and RH lines, expression levels of *PR* genes in *ZmFBL41*-overexpressing plants, *zmfbl41* and *zmcad* mutants, disease index of W22, *zmfbl41* and *zmcad* mutants, lesion length of *ZmFBL41*-overexpressing and *OsCAD8B* knockout plants, lignin content in SH and RH lines, *zmfbl41* and *zmcad* mutants and *OsCAD8B* knockout plants, and seedling height between Zhonghua 11 and *OsCAD8B* knockout plants.

Reporting Summary. Further information on research design is available in the Nature Research Reporting Summary linked to this article.

Data availability

Data supporting the findings of this work are available within the paper and its Supplementary Information. All materials used in this study have been described in previous studies[8,33,34]. The RNA-sequencing data for all 368 inbred lines have been

deposited in the NCBI Sequence Read Archive under accession code SRP026161. The genotype after imputation can be downloaded from http://www.maizego.org/Resources.html. The widely used mapping population, although not owned by us, can—to our knowledge—be accessed by any researcher through appropriate application. Most of the data are from the GenBank of CIMMYT (details in Supplementary Table 1), which are public available, others can be obtained from the National GenBank, Institute of Crop Germplasm Resources of Chinese Academy of Agricultural Sciences (CAAS, http://www.cgris.net) with an MTA. The researchers can also contact the founders of lines of the mapping population (J.Y., yjianbing@mail.hzau.edu.cn). Source data for Figs. 3a,c, 5,a,c,e and Supplementary Figs. 1a, 2c, 6e,f have been provided in Supplementary Table 8.

References

73. Bradbury, P. J. et al. TASSEL: software for association mapping of complex traits in diverse samples. *Bioinformatics* **23**, 2633–2635 (2007).
74. Chen, S., Songkumarn, P., Liu, J. & Wang, G. A versatile zero background T-vector system for gene cloning and functional genomics. *Plant Physiol.* **150**, 1111–1121 (2009).
75. Yang, F. et al. Functional analysis of the *GRMZM2G174449* promoter to identify *Rhizoctonia solani*-inducible *cis*-elements in maize. *BMC Plant Biol.* **17**, 233 (2017).
76. Ma, X. & Liu, Y.-G. CRISPR/Cas9-based multiplex genome editing in monocot and dicot plants. *Curr. Protoc. Mol. Biol.* **115**, 31.6.1–31.6.21 (2016).

nature research

Corresponding author(s): Zhaohui Chu

Last updated by author(s): Aug 17, 2019

Reporting Summary

Nature Research wishes to improve the reproducibility of the work that we publish. This form provides structure for consistency and transparency in reporting. For further information on Nature Research policies, see Authors & Referees and the Editorial Policy Checklist.

Statistics

For all statistical analyses, confirm that the following items are present in the figure legend, table legend, main text, or Methods section.

n/a	Confirmed	
☐	☒	The exact sample size (*n*) for each experimental group/condition, given as a discrete number and unit of measurement
☐	☒	A statement on whether measurements were taken from distinct samples or whether the same sample was measured repeatedly
☐	☒	The statistical test(s) used AND whether they are one- or two-sided *Only common tests should be described solely by name; describe more complex techniques in the Methods section.*
☒	☐	A description of all covariates tested
☒	☐	A description of any assumptions or corrections, such as tests of normality and adjustment for multiple comparisons
☐	☒	A full description of the statistical parameters including central tendency (e.g. means) or other basic estimates (e.g. regression coefficient) AND variation (e.g. standard deviation) or associated estimates of uncertainty (e.g. confidence intervals)
☐	☒	For null hypothesis testing, the test statistic (e.g. *F*, *t*, *r*) with confidence intervals, effect sizes, degrees of freedom and *P* value noted *Give P values as exact values whenever suitable.*
☒	☐	For Bayesian analysis, information on the choice of priors and Markov chain Monte Carlo settings
☒	☐	For hierarchical and complex designs, identification of the appropriate level for tests and full reporting of outcomes
☒	☐	Estimates of effect sizes (e.g. Cohen's *d*, Pearson's *r*), indicating how they were calculated

Our web collection on statistics for biologists contains articles on many of the points above.

Software and code

Policy information about availability of computer code

Data collection	No software was used.
Data analysis	GWAS was performed in TASSEL 3.0.

For manuscripts utilizing custom algorithms or software that are central to the research but not yet described in published literature, software must be made available to editors/reviewers. We strongly encourage code deposition in a community repository (e.g. GitHub). See the Nature Research guidelines for submitting code & software for further information.

Data

Policy information about availability of data

All manuscripts must include a data availability statement. This statement should provide the following information, where applicable:

- Accession codes, unique identifiers, or web links for publicly available datasets
- A list of figures that have associated raw data
- A description of any restrictions on data availability

Data supporting the findings of this work are available within the paper and its Supplementary Information files. All the materials used in this study have been well described in previous studies (Yang X et al., Mol Breed, 2001, cited in ref. 33; Li H et al., Nat Genet, 2013, cited in ref. 8; Fu J et al., Nat Commun, 2013, cited in ref. 34). The RNA-sequencing data for all the 368 inbred lines has been deposited in the NCBI Sequence Read Archive under accession code SRP026161. The genotype after imputation can be downloaded from the website http://www.maizego.org/Resources.html. The mapping population has been widely used in the world with about 30 papers published, we believe that any researcher can accessed them with the appropriate approach. In fact, we are not the owners of these materials, but obtained them based on the published articles. Most of them are from the GenBank of CIMMYT (detail in the supplementary table 1) which are public available, others can be obtained from the National GenBank, Institute of Crop Germplasm Resources of Chinese Academy of Agricultural Sciences (CAAS, http://www.cgris.net) with the MTA. The researchers can also contact the founder of this population (Jianbing Yan, yjianbing@mail.hzau.edu.cn; Jiansheng Li, and Xiaohong Yang). Source data for Figs 3a, c, 5a, c, e and Supplementary Figs 1a, 2c have been

provided in Supplementary Table 8 -Statistic Source Data.

Field-specific reporting

Please select the one below that is the best fit for your research. If you are not sure, read the appropriate sections before making your selection.

☒ Life sciences ☐ Behavioural & social sciences ☐ Ecological, evolutionary & environmental sciences

For a reference copy of the document with all sections, see nature.com/documents/nr-reporting-summary-flat.pdf

Life sciences study design

All studies must disclose on these points even when the disclosure is negative.

Sample size	318 maize inbred lines were chosen to perform GWAS, because many genes were successfully cloned using this population previously. Three transgenic lines and 10 plants of each lines were chosen because this sample size was sufficient to perform statistical analysis.
Data exclusions	No data were excluded from the analyses.
Replication	All attempts at replication were successful.
Randomization	The samples were allocated into experimental groups randomly.
Blinding	The investigators were blinded to group allocation during data collection and analysis.

Reporting for specific materials, systems and methods

We require information from authors about some types of materials, experimental systems and methods used in many studies. Here, indicate whether each material, system or method listed is relevant to your study. If you are not sure if a list item applies to your research, read the appropriate section before selecting a response.

Materials & experimental systems

n/a	Involved in the study
☐	☒ Antibodies
☒	☐ Eukaryotic cell lines
☒	☐ Palaeontology
☒	☐ Animals and other organisms
☒	☐ Human research participants
☒	☐ Clinical data

Methods

n/a	Involved in the study
☒	☐ ChIP-seq
☒	☐ Flow cytometry
☒	☐ MRI-based neuroimaging

Antibodies

Antibodies used	Mouse monoclonal anti-Myc Tag, Abcam, Ab18185; Mouse monoclonal anti-β-Actin, CWBIO, CW0264M; Mouse monoclonal anti-HA, Abcam, Ab1424; Mouse monoclonal anti-MBP, CWBIO, CW0288M
Validation	Mouse monoclonal anti-Myc Tag and mouse monoclonal anti-HA antibodies were used in Co-IP, mouse monoclonal anti-β-Actin and mouse monoclonal anti-MBP antibodies were used to detect protein stability.